Research Article Vol. 62, No. 7 / 1 March 2023 / Applied Optics B79

applied optics

Broadband infrared absorber based on a sputter deposited hydrogenated carbon multilayer enhancing MEMS-based CMOS thermopile performance

Sam Ahmadzadeh,[1,2,*] Des Gibson,[1,3] Lewis Fleming,[1,3] David Hutson,[1,3] Shigeng Song,[1,3] Allan James,[2] Stephen Wells,[2] Alan Forsyth,[2] and Suzanne Bruckshaw[2]

[1]Institute of Thin Films, Sensors and Imaging, Scottish Universities Physics Alliance School of Computing, Engineering and Physical Sciences, University of the West of Scotland, Paisley PA12BE, Scotland, UK
[2]Semefab Ltd., Newark Road South, Eastfield Industrial Estate, Glenrothes KY7 4NS, Scotland, UK
[3]Albasense Ltd., Paisley PA1 2BE, Scotland, UK
*Corresponding author: sam.ahmadzadeh@uws.ac.uk

Received 30 September 2022; revised 24 November 2022; accepted 24 November 2022; posted 1 December 2022; published 5 January 2023

Based on pulsed DC sputter deposition of hydrogenated carbon, an absorber optical coating with maximized broadband infrared absorptance is reported. Enhanced broadband (2.5–20 μm) infrared absorptance (>90%) with reduced infrared reflection is achieved by combining a low-absorptance antireflective (hydrogenated carbon) overcoat with a broadband-absorptance carbon underlayer (nonhydrogenated). The infrared optical absorptance of sputter deposited carbon with incorporated hydrogen is reduced. As such, hydrogen flow optimization to minimize reflection loss, maximize broadband absorptance, and achieve stress balance is described. Application to complementary metal-oxide-semiconductor (CMOS) produced microelectromechanical systems (MEMS) thermopile device wafers is described. A 220% increase in thermopile output voltage is demonstrated, in agreement with modeled prediction.

https://doi.org/10.1364/AO.477050

1. INTRODUCTION

Thermopiles are a type of thermal detector that have benefits of low cost, broadband spectral response, and simplicity of use. In industrial settings, microelectromechanical systems (MEMS) based thermopile technologies are utilized within noncontact thermometry, thermal flow sensors, and nondispersive infrared (NDIR) gas sensors aimed at CO_2 and CH_4 and thermal imagers [1]. As shown in the following figure, the thermopile chip consists of a silicon substrate, membrane structure, thermopile, and broadband absorber layer.

On exposure to IR radiation, a temperature difference, ΔT, is observed between hot and cold junctions. The resulting thermoelectric differential is transformed into an electrical output; this direct conversion is known as the Seebeck effect [2]. The absorptance of the incident infrared radiation by the thermopile device results in enhanced output voltage. Silicon is extensively used in MEMS-based thermopile devices due to its low cost and compatibility with complementary metal-oxide-semiconductor (CMOS) wafer processing [3].

Applying a high-absorptance porous metal coating to the detector active area is a standard method to achieve broadband absorptance, with numerous articles published describing such "metal black" coatings, often referred to as gold-black, silver-black, and platinum-black [4–6]. However, the porous metal coatings are typically high cost, easily damaged, and are not compatible with CMOS processing. Furthermore, the process of "metal-black" coating is more complex than other techniques and can cause the thermopile device to be fragile for next-stage photolithography and etch process steps [4].

A silicon nitride (Si_3N_4) or silica (SiO_2) layer or $SiO_2/Si_3N_4/SiO_2$ sandwich film structure is also often used as the thermopile IR absorber, termed a "membrane" layer, as shown in Fig. 1. However, the membrane layer provides low IR absorptance and narrow absorptance range [4,7–9].

This paper provides a new CMOS-compatible durable broadband absorber (BBA) multilayer optical coating based on a hydrogenated carbon two-layer structure, overcoming shortfalls of the metal-black and Si_3N_4/SiO_2 multilayer absorber approaches. Deposition utilizes pulsed DC sputtering of carbon with controlled hydrogenation during sputtered carbon deposition. Combining a broadband absorptance carbon layer (nonhydrogenated) with a low absorptance antireflective

(hydrogenated carbon) overcoat provides broadband (2.5–20 μm) IR absorptance (>90%) with minimal IR reflection. The deposition process involves room-temperature pulsed DC deposition of carbon with controlled introduction of hydrogen during the carbon deposition [10]. This approach provides control of the spatial absorptance distribution through the carbon coating, thereby achieving an optimized combination of reduced reflectance and maximized absorptance [11].

2. THEORY

The incident IR radiation absorbed by the BBA multilayer creates a thermal gradient between the hot and cold junctions of the thermopile, shown as ΔT in Fig. 1. This produces a thermoelectric voltage and is directly related to the Seebeck effect, absorber efficiency, and number of thermocouples used.

The voltage output shown in Fig. 1 can be calculated using the number of thermopiles in a serially connected configuration and the Seebeck effect coefficients for the material used [4]. Calculation of output voltage is provided as follows:

$$\text{Output voltage} = N\Delta T\,|\alpha_A - \alpha_B| = N\Delta T\alpha_{AB}, \quad \textbf{(1)}$$

where N is number of serially connected thermocouples and the Seebeck coefficients for materials A and B are denoted by α_A and α_B, respectively, and $\alpha_{AB} = |\alpha_A - \alpha_B|$ is the relative Seebeck coefficient. The thermal gradient and temperature difference between the hot and cold junctions is expressed as follows [4]:

$$\Delta T = \frac{\eta P_o}{G_{\text{th}}}, \quad \textbf{(2)}$$

where the IR absorptance of the material is denoted by η, the total thermal conductivity of detector denoted by G_{th} and incident power denoted by P_0. Substituting Eq. (2) into Eq. (1):

$$\text{Output voltage} = N\frac{\eta P_o}{G_{\text{th}}}\,|\alpha_A - \alpha_B| = N\frac{\eta P_o}{G_{\text{th}}}\alpha_{AB}. \quad \textbf{(3)}$$

Therefore, the voltage output is proportional to the absorptance (η). η is wavelength-dependent and as such has to be optimized over the required spectral range [4].

3. MODELING

Essential Macleod optical coating design software [12] was used to model and optimize the thickness of the carbon coating and

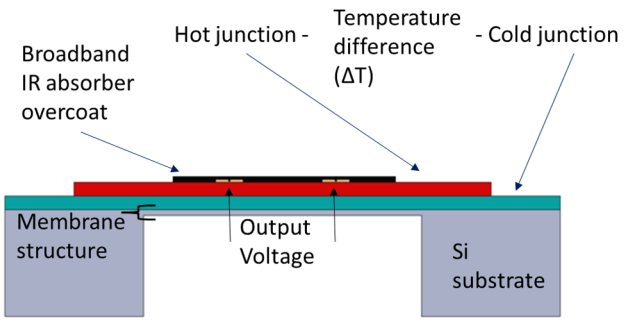

Fig. 1. Thermopile chip consisting of silicon substrate, membrane structure, thermopile, broadband absorber layer, and broadband antireflective match layer 2.

Table 1. Table of Membrane Structure, Materials, and Layer Thicknesses

Layer Material	Physical Thickness (nm)
Si_3N_4	600
SiO_2	450
Si_3N_4	170
SiO_2	570
Si_3N_4	110

Table 2. Table of Membrane Structure + BBA Coating Materials and Thicknesses

Material	Physical Thickness (nm)
Hydrogenated carbon (AR layer)	636
Nonhydrogenated carbon (absorber layer)	2000
Si_3N_4	600
SiO_2	450
Si_3N_4	170
SiO_2	570
Si_3N_4	110

resulting absorptance on top of the membrane structure. The membrane is a Si_3N_4/SiO_2 alternating layer structure [8], as presented in Table 1. Modeled absorptance for Si_3N_4/SiO_2 membrane gives an average value of 42.73% over a 2.5–20 μm spectral range, as shown in Fig. 2.

Single layers of carbon deposited with varying hydrogen flow were examined in a previous publication for optical stress and mechanical performance [10]. Essential Macleod software was used to fit measured data using the envelope fitting method for optical constant extraction, n, and k. The returned optical constants from Essential Macleod at the half- and quarter-wave turning points were fit to a Cauchy model [13] to obtain smooth (values in between the wavelengths are derived using linear interpolation) n/k data over the desired range. The smoothed optical constant data were used to model a multilayer carbon thin film with desired absorptance at varying thicknesses.

Using the single layer results, an optical coating design model was generated to optimize the carbon topcoat thickness (consisting of absorber and antireflection [AR] layer shown in Fig. 3) and predicting the absorbance response AR layer used to increase the throughput by reducing the reflection to maximize overall performance boost. The optimized thickness output from the model is presented in Table 2 and schematic shown in Fig. 3. The carbon bilayer in the below table is termed the broadband absorber (BBA) multilayer optical coating.

When comparing the modeled results for the membrane without and with BBA overcoat, a significant enhancement in broadband absorptance is demonstrated. The boost shown in Fig. 2, which shows modeled performance, demonstrating the best result and a factor of 2.2× performance enhancement (average spectral absorptance of coated and uncoated Si_3N_4/SiO_2 membrane, 93.81% and 42.73%, respectively). Table 2 provides the layer structure of membrane layers with optimized carbon multilayer overcoat.

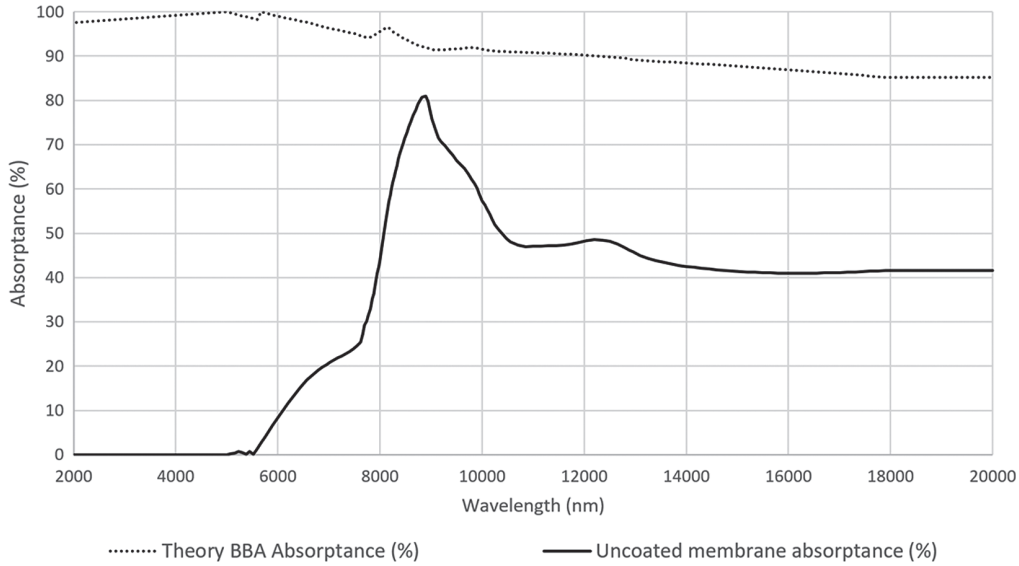

Fig. 2. Modeled absorptance for Si_3N_4/ SiO_2 membrane and BBA overcoat layer.

4. EXPERIMENTAL RESULTS

A. Deposition

Deposition was carried out using a pulsed DC sputtering process. The deposition system uses a horizontal-axis rotating drum in which deposition of each layer can be achieved with multiple passes across a rectangular planar DC magnetron source; substrates are mounted on removable drum plates. A schematic of the drum-based sputter deposition system configuration with two 6 in. wafers per plate, with two populated plates, is shown in Fig. 4. The system shown in Fig. 4 can accommodate 40 × 6 in. silicon wafers per deposition run.

A final system-based pressure of 5×10^{-7} mbar is achieved by a combination of turbo (Pfeiffer Vacuum D-35614 asslar turbomolecular pump, 2200 L/s) and cryocooler water vapor pumping (Telemark Cryogenics/3600 Model). Controlled hydrogen introduction is via a high-purity hydrogen generator (Linde/NMH, 500 model) using water electrolysis [14]. To ensure the desired coating aesthetic quality, pulsed DC sputtering is used to minimize arcing. Table 3 shows the typical deposition parameters used. There was no direct substrate heating, and all depositions were carried out at room temperature.

Deposited carbon film thickness uniformity achieved across two wafers per plate, as shown in Fig. 4, is ±5%.

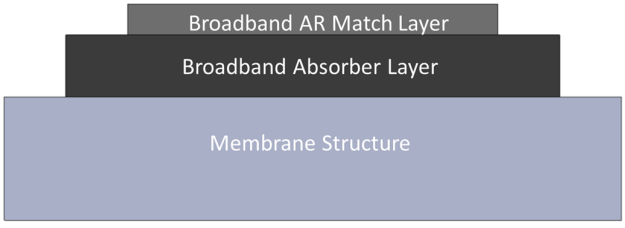

Fig. 3. Schematic of the layer structure of BBA overcoat.

Fig. 4. Photo of drum-based pulsed DC sputter system.

Table 3. Typical Deposition Conditions of Pulsed DC Sputtered Hydrogenated Carbon

Ar Flow (sccm)	H_2 Flow (sccm)	Power (kW)	Current (A)	Voltage (V)	Pulsed DC Frequency (kHz)	Pulse Length (μs)
100	0 to 5 sccms	4	10	400	66	4

B. Optical Measurements

Deposition of the modeled multilayer design was carried out, and spectral absorptance measurements, as shown in Fig. 5, were carried out using a Perkin Elmer 983 spectrophotometer, demonstrating broadband absorptance used to enhance output voltage MEMS thermopile chip performance.

For all coated substrates, the relationship among spectral transmittance, reflectance, and hydrogen flow was studied using Nicolet iS50 Fourier transform and Perkin Elmer 983 G infrared spectrophotometers, respectively. Spectral absorptance

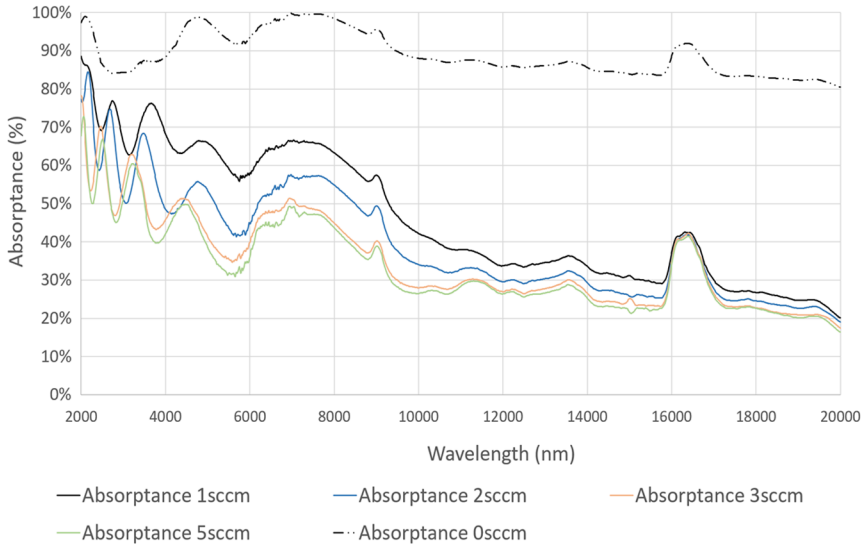

Fig. 5. Absorptance spectrum (2000 to 20,000 nm) for 0–5 sccm hydrogen flows.

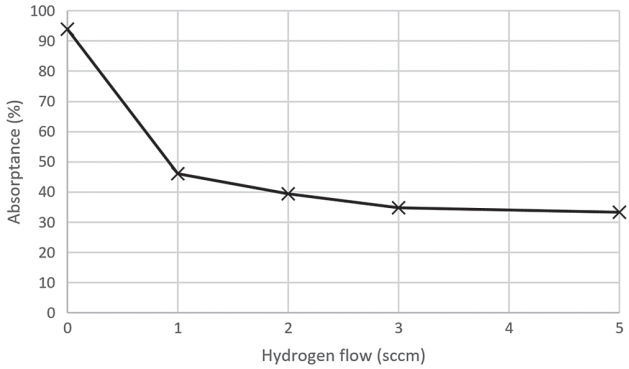

Fig. 6. Average absorptance over 2.5–20 μm range with varying hydrogen, 0–5 sccm, within the absorber layer, for the full multilayer carbon absorber.

was calculated from the spectral transmittance and reflectance results and is as shown in Fig. 5.

From the results of depositions, as shown in Fig. 5, the non-hydrogenated (0 sccm) offers the max absorbance across the 2.5–20 μm range with average absorptance of 94.14%. As the hydrogenation is increased from 0°–5 sccm, a trend of reducing absorptance is observed. This trend is due to hydrogen incorporation into the sputter deposited carbon significantly decreasing infrared optical absorptance due to a decrease in deep absorptive states associated with dangling bonds [10,11,15].

Figure 6 demonstrates the average absorptance and hydrogen relationship; as hydrogen is increased, the average absorptance drops with a maximum at no hydrogen (0 sccm) of 94.14% and a minimum at 5 sccm flow hydrogen during deposition at 33.38%. This highlights that a 0 sccm absorber layer is the best performing as an absorber layer to enhance thermopile chip performance.

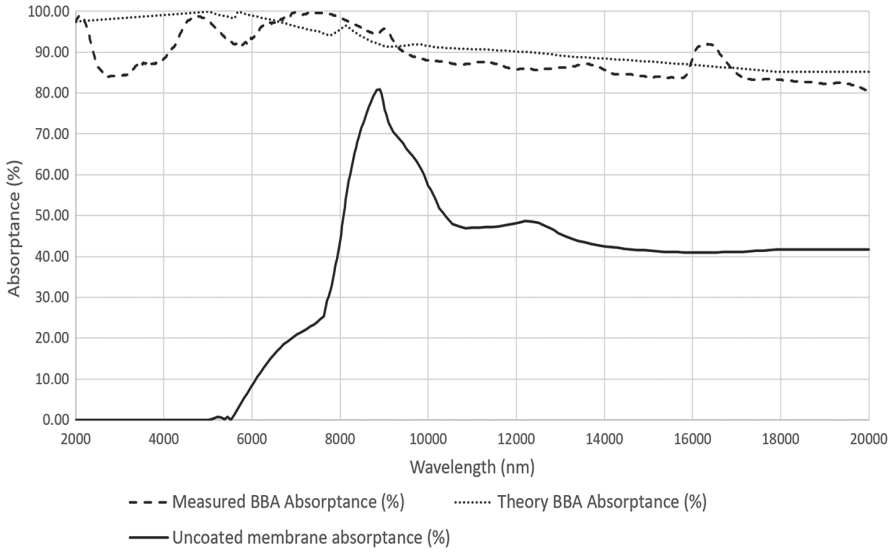

Fig. 7. Comparison of modeled and measured BBA coating.

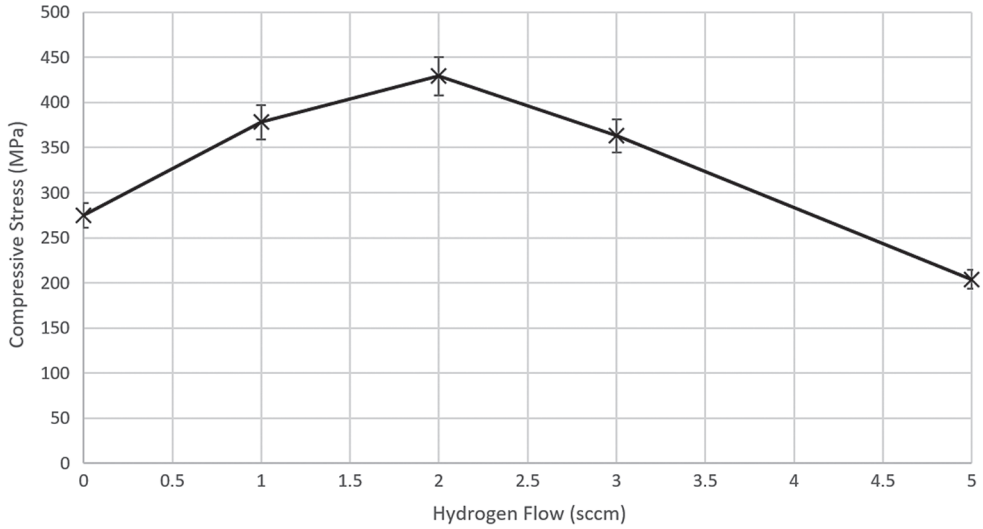

Fig. 8. Full absorber multilayer coating design with varying hydrogen flows, 0–5 sccm, within the absorber layer and measured stress with error bars [17].

Table 4. Campaign of Test Runs with Varying Hydrogen Flow in the Absorber Layer and Associated Stress Results

Hydrogen Flow Absorber Layer (sccm)	Thickness Measured by SEM (μm)	|AVG Stress| (MPa)	|CNT Stress| (MPa)
0	2.81	275	241
1	2.55	378	349
2	2.63	429	346
3	2.91	363	304
5	3.20	204	185

Comparing the experimentally deposited BBA coating with the modeled spectral response, as shown in Fig. 7, good agreement is demonstrated with an achieved average spectral absorptance (2.5–20 μm) of 94.1%.

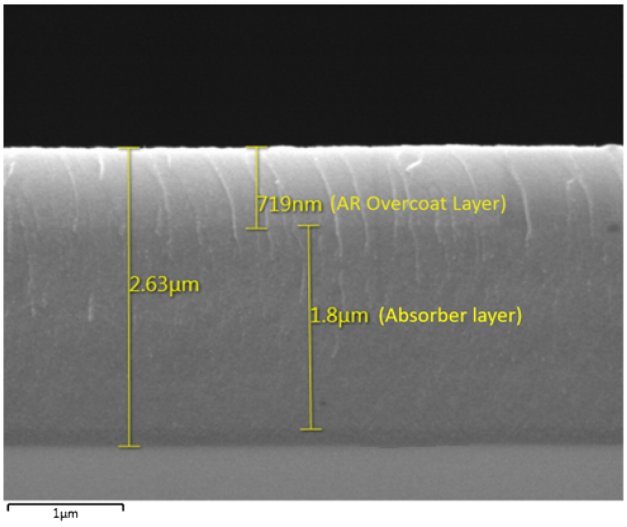

Fig. 9. Electron micrograph showing a typical BBA cross section with AR and absorber layers detailed.

C. Stress

Average stress was investigated as a function of hydrogen flow from 0–5 sccm for the absorber layer (nonhydrogenated) within the full multilayer carbon absorber coating design.

The change in curvature of an elastically deformed coated substrate (150 mm in diameter and 300 μm thick silicon wafer) is used to calculate the average film stress. The Stoney formula is used to determine stress [16]. Wafer geometry was measured before and after coating deposition using a capacitive distance sensor gauge made by E + H metrology GmbH (model MX- 203-6-33). Based on the Stoney formula, the machinery automatically determines the coating stress [16].

Results are shown in Table 4 and Fig. 8, indicating pulsed DC sputtered carbon BBA stress with varying hydrogen. The stress is compressive and peaks 2 sccm at a max value of 429 MPa average stress. With increasing hydrogen above 2 sccm, the stress is reduced to 204 MPa at 5 sccm. At 0 sccm, the resulting stress level is the second-lowest value recorded at 275 MPa compressive stress. Figure 9 shows a typical BBA cross section with AR and absorber layers as designed and presented in Fig. 3.

D. Absorptance/Stress Relationship and Optimization

The absorptance value ranges from 94.1% to 33.4% with increasing hydrogen flow. Nonhydrogenated (0 sccm) offers the best result for enhancing the thermopile chip performance. The compressive thin film stress value is more complicated in that a maximum is reached at 2 sccm flow and dropping hydrogen at highest and lowest flows tested, 0 and 5 sccm, respectively.

Comparing the stress and absorptance results, the nonhydrogenated 0 sccm absorber layer offers the best compromise between low compressive stress and high absorptance in BBA coating used to boost thermopile chip. This is illustrated in Fig. 10, when considering both stress and absorptance, nonhydrogenated (0 sccm) offers the highest absorptance and second-lowest compressive stress value.

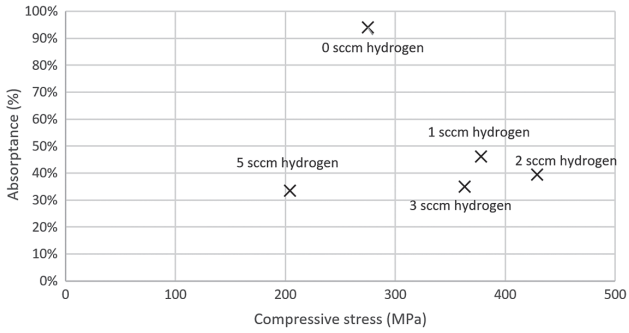

Fig. 10. Absorptance as a function of compressive stress for the absorber multilayer with varying hydrogen flow.

5. TESTING: THERMOPILE CHIPS

A thermopile chip without and with best-performing BBA multilayer optical coating underwent output voltage performance testing at five sites on a 6 in. silicon wafer, as shown in Fig. 11, positioned on the wafer center, east, north, south, and west, as shown in Fig. 11.

Testing coated and uncoated thermopiles utilized a broadband blackbody IR source (2.5 to 20 μm), exposed to the blackbody IR source (Yangzhou Tuanrui Electric Co., Ltd/High temperature ceramic heating plate) and output voltage measured, as shown in Fig. 12. The output voltages are presented in Table 5.

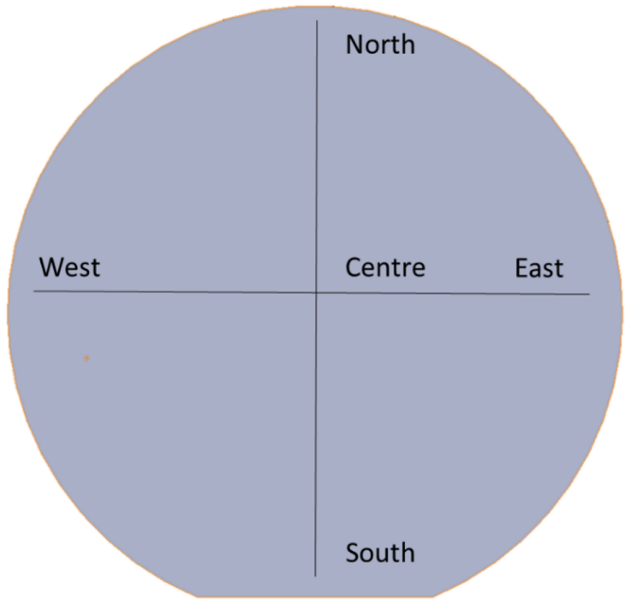

Fig. 11. Schematic of sites center, east, north, south, and west on 6 in. silicon wafer.

The output voltage for uncoated and coated thermopile chip results in a 220% increase in response in agreement with modeled prediction.

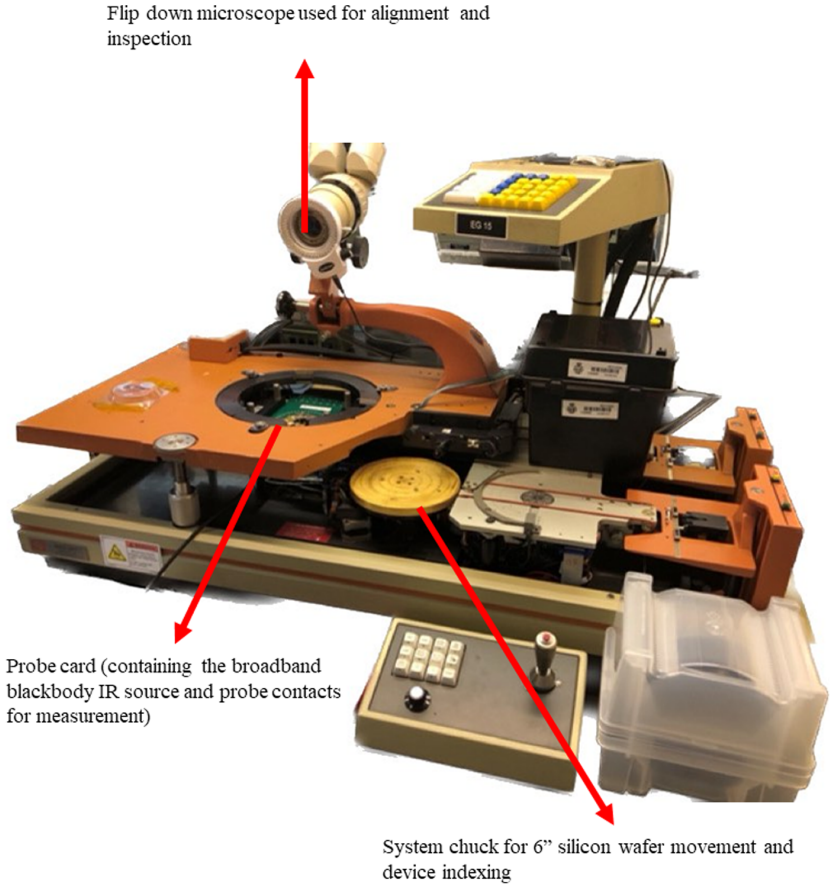

Fig. 12. Experiment setup of the thermopile chip voltage output measurement.

Table 5. Results of Full Device Wafer Testing Performed under a Broadband IR Source on Coated and Uncoated Die

Site on Wafer	Absorber Thermopile Voltage Output -Va (mV)	No Absorber Thermopile Voltage Output - Vn (mV)	Percentage Boost at Sites	Average Percentage Boost Across All Sites
Centre	391.55	196.88	198%	220%
East	329.55	168	196%	
North	372.22	185.33	200%	
South	260.88	104	250%	
West	285.11	112	254%	

Table 6. Correlation between Coated and Uncoated Die

Calculation	Membrane	Membrane with BBA
Standard deviation	18.03	20.7
Average percentage standard deviation	12%	6%

The correlation between coated and uncoated die shows the carbon absorber coating systematically boosts uncoated die at each of the five positions, and the variation measured between sites is due to initial variability in noncoated die. Average voltage variation and percentage standard deviation between absorber coated and nonabsorber coated devices shows a spread of 6% and 12%, respectively, indicating the BBA acts to reduce the spread of output voltages and stabilize the thermopile devices and output voltages, which is shown in Tables 5 and 6.

6. CONCLUSION

In this work, pulsed DC high-throughput drum-based sputtering is employed to deposit a hydrogenated carbon optical coating, termed a BBA multilayer. The BBA multilayer was deposited onto MEMS-based CMOS thermopile devices, fabricated on 6 in. diameter silicon wafers. The BBA multilayer structure is a two-layer patented [11] design comprising a low absorptance antireflective (hydrogenated carbon) overcoat with a broadband absorptance carbon underlayer (nonhydrogenated). The BBA multilayer provides enhanced broadband (2.5–20 μm) infrared absorptance (>90%) with minimal infrared reflection.

Results from modeling of the BBA structure deposited on the silicon membrane structure, described in Section 2, predicted a 220% boost in output voltage. This boost was verified by measuring uncoated (average spectral absorptance $[2.5-20\ \mu\text{m}] = 42.7\%$) and BBA-coated (average spectral absorptance $[2.5-20\ \mu\text{m}] = 94.14\%$) thermopile devices.

The influence of increasing hydrogen is a reduction in infrared optical absorptance. The decreasing infrared optical absorptance is due to a decrease in deep absorptive states associated with dangling bonds, reducing their concentration from typically 10^{19} to 10^{16} cm^{-3} [15]. Increasing hydrogen content reduction in compressive stress is observed with a minimum measured stress of 204 MPa at 5 sccm hydrogen flow.

As a result, increasing hydrogen content of the BBA coating significantly decreases broadband absorptance, while significantly reducing compressive stress for hydrogen flow greater than 4 sccm flow. A peak stress is reached at 2 sccm flow in the absorber layer with a value of 429 MPa. As such, a compromise between thin film compressive stress and absorptance is required.

In addition to overall boost of thermopile device output voltage, the BBA coating reduces spread of the output voltages across the 6 in. silicon device wafer's surface.

Funding. Innovate UK Knowledge Transfer Partnership Program (KTP) (104736); Semefab Ltd.

Acknowledgment. We would like to thank Angus Airlie for his valued technical support throughout the duration of this work.

Disclosures. The authors declare no conflicts of interest.

Data availability. Data underlying the results presented in this paper are not publicly available at this time but may be obtained from the authors upon reasonable request.

REFERENCES

1. S. Udina, M. Carmona, G. Carles, J. Santander, L. Fonseca, and S. Marco, "A micromachined thermoelectric sensor for natural gas analysis: thermal model and experimental results," Sens. Actuators B Chem. **134**, 551–558 (2008).
2. H. Liu, W. Sun, and S. Xu, "An extremely simple thermocouple made of a single layer of metal," Adv. Mater. **24**, 3275–3279 (2012).
3. J.-K. Chang, H. Fang, C. A. Bower, E. Song, X. Yu, and J. A. Rogers, "Materials and processing approaches for foundry-compatible transient electronics," Proc. Natl. Acad. Sci. **114**, E5522–E5529 (2017).
4. H. Hou, Q. Huang, G. Liu, and G. Qiao, "Enhanced performances of CMOS-MEMS thermopile infrared detectors using novel thin film stacks," Infrared Phys. Technol. **102**, 103058 (2019).
5. S. Ahmadzadeh, D. Gibson, L. Fleming, D. Hutson, G. Mcgann, S. Song, A. Belke, A. James, S. Wells, A. Forsyth, and S. Bruckshaw, "Broadband infrared absorber based on a sputter deposited hydrogenated carbon multilayer enhancing MOEMS based CMOS thermopile performance," in *Optical Interference Coatings Conference (OIC)* (2022), paper MC.4.
6. M. Hirota, Y. Nakajima, M. Saito, and M. Uchiyama, "120×90 element thermoelectric infrared focal plane array with precisely patterned Au-black absorber," Sens. Actuators A Phys. **135**, 146–151 (2007).
7. R. Lenggenhager, H. Baltes, J. Peer, and M. Forster, "Thermoelectric infrared sensors by CMOS technology," IEEE Electron Device Lett. **13**, 454–456 (1992).
8. F. Jutzi, D. H. B. Wicaksono, G. Pandraud, N. de Rooij, and P. J. French, "Far-infrared sensor with LPCVD-deposited low-stress Si-rich nitride absorber membrane," Sensors Actuators A Phys. **152**, 126–138 (2009).
9. D. Xu, B. Xiong, and Y. Wang, "Design, fabrication and characterization of a front-etched micromachined thermopile for IR detection," J. Micromech. Microeng. **20**, 115004 (2010).
10. D. Gibson, S. Song, L. Fleming, S. Ahmadzadeh, H. O. Chu, S. Sproules, R. Swindell, X. Zhang, P. Navabpour, C. Clark, and M. Bailey, "Durable infrared optical coatings based on pulsed DC-sputtering of hydrogenated amorphous carbon (a-C:H)," Appl. Opt. **59**, 2731–2738 (2020).

11. D. Gibson, S. Song, and D. Hutson, "An absorber, a detector comprising the absorber and a method of fabricating the absorber," Patent Application GB2016210.3 (13 October 2020).
12. "Essential Macleod," 2022, https://www.thinfilmcenter.com/essential.php.
13. Thin Film Center Inc., *Essential Macleod - Optical Coating Design Program Manual, 11.5* (2019).
14. D. M. F. Santos, C. A. C. Sequeira, and J. L. Figueiredo, "Hydrogen production by alkaline water electrolysis," Quim. Nova **36**, 1176–1193 (2013).
15. W. Beyer, "Hydrogen phenomena in hydrogenated amorphous silicon," in *Semiconductors and Semimetals* (1999), Chapter 5, pp. 165–239.
16. G. G. Stoney, "The tension of metallic films deposited by electrolysis," Proc. R. Soc. London. Ser. A **82**, 172–175 (1909).
17. E+H Metrology GmbH, *Wafer Geometry Gauge MX 203-6-33—Manual* (2017), Vol. **V100**.